A convective–radiative propagation model for wildland fires

Jacques Henri Balbi, François Joseph Chatelon, Dominique Morvan, Jean Louis Rossi, Thierry Marcelli, Frédéric Morandini

A convective–radiative propagation model for wildland fires

Jacques Henri Balbi[A], *François Joseph Chatelon*[A], *Dominique Morvan*[B], *Jean Louis Rossi*[A], *Thierry Marcelli*[A,C] *and Frédéric Morandini*[A]

[A]Université de Corse, Systèmes Physiques pour l'Environnement UMR-CNRS 6134, Campus Grossetti, BP 52 20250 Corte, France.
[B]Aix Marseille Université, Centre National de la Recherche Scientifique, Centrale Marseille, M2P2, 13451 Marseille, France.
[C]Corresponding author. Email: marcelli@univ-corse.fr

Abstract. The 'Balbi model' is a simplified steady-state physical propagation model for surface fires that considers radiative heat transfer from the surface area of burning fuel particles as well as from the flame body. In this work, a completely new version of this propagation model for wildand fires is proposed. Even if, in the present work, this model is confined to laboratory experiments, its purpose is to be used at a larger scale in the field under operational conditions. This model was constructed from a radiative propagation model with the addition of a convective heat transfer term resulting from the impingement of packets of hot reacting gases on unburnt fuel elements located at the base of the flame. The flame inside the fuel bed is seen as the 'fingers of fire' described in the literature. The proposed model is physics-based, faster than real time and fully predictive, which means that model parameters do not change from one experiment to another. The predicted rate of spread is applied to a large set of laboratory experiments (through homogeneous pine needles and excelsior fuel beds) and is compared with the predictions of both a very simple empirical model (Catchpole) and a detailed physical model (FireStar2D).

Additional keywords: convective flux, fire dynamics, fire spread, heat transfer, model performance, radiative flux, physical model, steady-state model.

Introduction

Forest fire modelling uses several different approaches (reviewed by Sullivan 2009*a*, 2009*b*). According to the nature of the equations that describe wildland fire mathematical models, three kinds of modelling are usually used (Perry 1998): (1) empirical models exclusively determined using experimental data and not involving any physical mechanisms (McArthur 1966; Noble *et al.* 1980; Cheney *et al.* 1998); (2) semi-physical models based on the energy conservation principle, without distinction between heat transfer modes. The best known is the one proposed by Rothermel (1972); (3) physical models that differentiate between the various types of heat transfer (Pagni and Peterson 1973; Albini 1985; Grishin 1997; Balbi *et al.* 2007; Morvan *et al.* 2013). So mathematical relationships are generated from the laws that govern fluid mechanics, combustion and heat transfer using fuel characteristics, terrain topography and weather conditions.

The question about the dominant heat transfer mode remains unanswered among the scientific community: is the propagation of wildfires driven by convection, radiation or both? Radiation and convective heat transfer have been widely studied in the literature. Some authors have chosen to neglect convective effects, either for the sake of simplification or owing to experimental conditions in which flame radiation is assumed to be dominant (Albini 1982; Catchpole *et al.* 2002; Balbi *et al.* 2010). The question about the role of convective heat transfer has been discussed by Pagni and Peterson (1973) and they found convection to be the primary heat transfer mechanism under some conditions. For specific fuel beds (for instance discontinuous fuel beds), Weber (1990), Finney *et al.* (2006) and Chatelon *et al.* (2017) suggested that convective heat transfer is necessary for fire spread and is related to flame dynamics, and some recent works (Morandini *et al.* 2014, 2018; Grumstrup *et al.* 2017; Sánchez-Monroy *et al.* 2019) investigated the relevance of convective *v.* radiative flux. Moreover, the main well-known computational fluid dynamics (CFD)-based physical models (e.g. FireStar3D (Morvan *et al.* 2018), FIRETEC (Linn and Cunningham 2005), FireFoam (El Houssami *et al.* 2016), WFDS, Wildland-Urban Interface Fire Dynamics Simulator, (Mell *et al.* 2009)) include both radiation and convective heat transfer modes.

The main goal of the present work is to propose a physical fire spread model at laboratory scale that considers both radiative and convective effects. This model has to be simple, robust

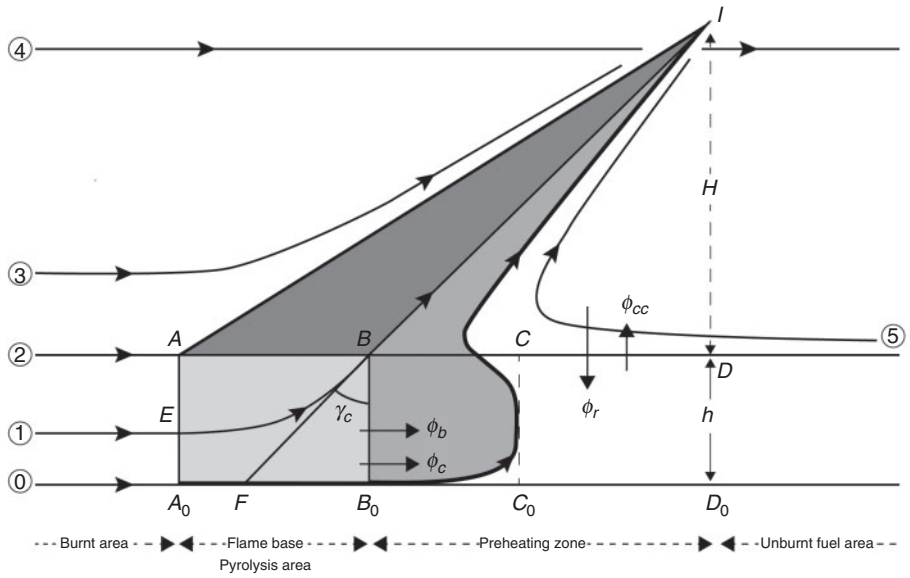

Fig. 1. A qualitative representation of the flaming zone combustion profile and streamlines.

and faster than real time in order to be used at field scale under operational conditions. The model is built as a combination of a radiative-only model (Balbi *et al.* 2009, 2010) and a convective model (Chatelon *et al.* 2017). The first section presents the main equations of the proposed model. In the second part, the radiative–convective model is applied to a large set of fires conducted at laboratory scale (Catchpole *et al.* 1998).

Model development

Simplified gas flow modelling

Even if the gas flow turbulence in the vicinity of a fire front is variable, its effect on spread is deterministic and following Chatelon *et al.* (2017), it can be represented by an equivalent average steady-state flow.

The flaming zone is split into two main parts. The flame base (delimited by points ABB_0A_0 on Fig. 1) represents the burning fuel particles area where pyrolysis gases are mixed with fresh air coming from the back of the fire front. Fresh air enters the flame base through interface AA_0 with a velocity equal to wind velocity U and is gradually slowed down owing to drag forces. It should be noted that wind velocity U may be a combination of ambient natural wind and fire-induced airflow (see details in Appendix A). Moreover, the temperature of pyrolysis gases (mixed with air) is greater than ambient temperature, and then a gas packet is also subject to upward gas acceleration due to buoyancy. Thus, streamlines are parallel to the ground before entering the flame base and bend to the top of the vegetation stratum as they get closer to the burning–unburnt fuel interface. Some gas packets, subject to wind velocity and upward gas velocity, go out throught the top of the flame base. This gas flow creates the flaming zone above the vegetation stratum (delimited by points ABI on Fig. 1), which is called the flame body. However, some gas packets go out of the flame base through the burning fuel–unburnt fuel interface BB_0 and create a contact flame (delimited by points BB_0C_0CI on Fig. 1). These two zones of gas packets are separated by streamline 1 on Fig. 1. This flame inside the fuel bed was described as 'fingers of fire' by Rothermel and Anderson (1966) and is the main cause of convective heat transfer. The convective preheating area is the zone delimited by points BB_0C_0C.

Flame tilt angle

Following Balbi *et al.* (2007, 2009), the flame tilt angle γ (see Fig. 2) is the result of a velocity composition vector law between the normal component of the wind velocity and upward gas velocity vector u:

$$\tan\gamma = \frac{U + u\sin\alpha}{u\cos\alpha} = \tan\alpha + \frac{U}{u\cos\alpha} \quad (1)$$

where α is the terrain slope angle. If u_0 denotes upward gas velocity at flame mid-height for a null slope, the term $u\cos\alpha = u_0$ only depends on fuel characteristics (Balbi *et al.* 2009). Finally, the expression for the flame tilt angle is the following:

$$\tan\gamma = \tan\alpha + \frac{U}{u_0} \quad (2)$$

Wind and slope effects on fire spread

At both laboratory and field scales, three situations are found:

- No wind and no slope conditions ($\gamma = 0$, $\alpha = 0$). The flame is usually vertical with $\gamma = 0$ (Rossa 2017). The flame creates an indraught coming from the burnt zone, U', and another coming from the unburnt zone U (see Fig. 2. In this case, U only represents the fire-generated inflow). They are usually equal even if in some, the flame is tilted towards the burnt zone ($U > U'$, $\gamma < 0$) as a backfire (Rossa 2017). Albini (1986) proved that convective cooling U' must be taken into account in order to obtain good agreement between predicted

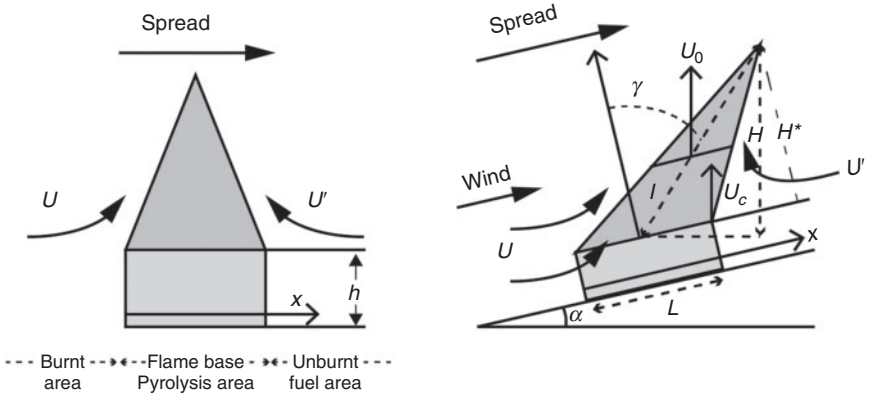

Fig. 2. Main physical characteristics of the fire front and related gas flows.

rate of spread (ROS) and experimental ROS. In the same way, an assumption of the proposed model is that convective cooling is strong enough to cancel out flame body radiation, and thus, flame base radiation is the primary heat transfer mechanism.

- No wind with slope conditions ($\gamma = 0$, $\alpha > 0$). Convective heating U induced by the slope acts like ambient wind. Moreover, if the slope angle is greater than a threshold value, it may lead to a drastic change in fire behaviour and turn it into an eruptive fire (see details in Appendix A).
- Wind and slope conditions ($\gamma > 0$, $\alpha > 0$). Ambient wind velocity is sufficient to supply the flame with oxygen and includes induced flow. Both the flame body and flame inside the fuel bed provide energy to the unburnt fuel up to the ignition temperature. This energy is due to flame radiation, convection provided by the internal flow and flame puffing because of turbulent effects (at the top of the vegetation stratum). A simplifying assumption consists in the cancellation of this puffing energy by the induced flow U'. It is also assumed that convective cooling cancels out the radiative effects far from the flame and thus, under the flame body, only flame radiation and convective cooling and heating remain.

Energy contributions

Four sources of heat transfer are taken into account:

- Flame base radiation – The radiation from burning fuel particles, heated by the flame body, impinges on the unburnt fuel on a distance equal to the extinction depth δ. The definition of δ is related to the optical depth defined by De Mestre *et al.* (1989; see Appendix B). The flame base is assumed to be a black radiant panel and Stefan–Boltzmann modelling is used to describe the flame base radiative heat flux, denoted by ϕ_b.
- Flame radiation – The flame body is assumed to be a grey radiant panel. The flame radiative heat flux ϕ_r is defined following Balbi *et al.* (2007, 2009).
- Convective heating – The flame body is assumed to be laminar in its first half above the vegetation stratum, and then, it acts as a barrier to air flow. The higher part of the flame is discontinuous and turbulent. Thus, fresh air may cross the flame (streamline 4 on Fig. 1) but, on the one hand, the temperature of this moving air is much closer to ambient than flame temperature and, on the other hand, it is too far from the fuel bed and is not continuously in contact with the vegetation stratum. According to Chatelon *et al.* (2017), this air flow does not create a convective warming flow. The hot gas flow inside the flame base provides a great amount of energy to the unburnt fuel by contact. This flow was observed by Finney *et al.* (2015). The convective warming flux is denoted ϕ_c.
- Convective cooling – The fire generates an inflow of fresh air resulting from the draught caused by the hot gaseous combustion products moving upwards. This fresh air coming from the unburnt zone (in front of the flame) cools the fuel bed, which is warmed by flame radiation. One important assumption (Balbi *et al.* 2007, 2009, 2010) consists in balancing these two effects far from the flame. Beyond point D, flame radiation and convective cooling cancel out each other. Thus, it is assumed that flame radiation only impinges on the unburnt fuel straight under the flame.

The convective cooling generated by the fire enters underneath the flame. If the flame tilt angle is small, the convective preheated zone (BC in Fig. 1) will be greater than the radiative preheated zone (BD in Fig. 1). Then, convective cooling only exchanges energy with the semi-internal flame (limited by streamline 0 in Fig. 1). If the flame tilt angle is large ($BC < BD$ in Fig. 1), the cooling airflow will come into contact with the unburnt fuel. This modelling agrees with measurements obtained by Liu *et al.* (2015). Indeed, Liu *et al.* (2015) observed under no-wind and small slope angle conditions that the cooling flame-induced flow is close to zero. However, when the slope angle and thus flame tilt angle are large, convective cooling cannot be neglected and the tilting flame will be close to the fuel bed, which can lead to an eruptive fire (Viegas 2004), which is an unsteady phenomenon. The steady-state model proposed only considers cases where the flame attachment phenomenon does not appear. Then, the convective cooling flux ϕ_{cc} will not appear in the energy balance. It allows the preheating zone to be limited to the area BDD_0B_0.

Preheating balance

In the preheating zone (BDD_0B_0), radiative heat fluxes ϕ_b and ϕ_r and the convective heat flux ϕ_c dry the fuel and can warm the fuel bed up to ignition temperature T_i. The simplified preheating

balance (integrated on the preheating zone) can be written as follows (with notation used in Fig. 1):

$$\int_D^B \sigma C_p \frac{dT_v}{dt} dx + \int_D^B \sigma_w C_{pw} \frac{dT_w}{dt} dx - \int_D^B \frac{d\sigma_w}{dt} \Delta h \, dx = a_b \phi_b + a_c \phi_c + a_r \phi_r \quad (3)$$

where a_b, a_r and a_c denote scaling factors, Δh is the heat of latent evaporation and σ, T and C_p are fuel load, temperature and specific heat respectively. The definition of all symbols is given in Table 1. The first integral in Eqn 3 represents the energy necessary to increase the temperature of a dry vegetation cell from ambient temperature T_a to ignition temperature T_i. The second integral represents the energy necessary to bring the water in a vegetation cell to vaporisation temperature (during this phase, the vegetation cell temperature is lower than that of its water T_w. Indeed, the fuel water is located at the surface of a dead fuel cell and is directly impinged on by radiative and convective fluxes) and the third integral corresponds to water vaporisation.

Considering a steady-state regime, and denoting ROS as $R = dx/dt$, Eqn 3 becomes:

$$\sigma C_p R \int_D^B dT_v + \sigma_w C_{pw} R \int_D^B dT_w - \Delta h R \int_D^B d\sigma_w = a_b \phi_b + a_c \phi_c + a_r \phi_r$$

And, finally, as m denotes the fuel moisture content:

$$\sigma C_p R(T_i - T_a) + m\sigma C_{pw} R\left(T_{vap} - T_a\right) + m\sigma \Delta h \, R = a_b \phi_b + a_c \phi_c + a_r \phi_r \quad (4)$$

Eqn 4 can be rewritten in a very simple way:

$$R = R_b + R_c + R_r \quad (5)$$

with

$$R_b = a_b \frac{\phi_b}{\sigma q} \quad (6)$$

$$R_c = a_c \frac{\phi_c}{\sigma q} \quad (7)$$

$$R_r = a_r \frac{\phi_r}{\sigma q} \quad (8)$$

where q is the energy required for ignition (depending on T_{vap}, vapourisation temperature):

$$q = C_p(T_i - T_a) + m\left(\Delta h + C_{pw}\left(T_{vap} - T_a\right)\right) \quad (9)$$

Flame base radiative heat flux

The temperature of the burning fuel particles is assumed to be equal to the flame temperature. The burning fuel–unburnt fuel interface is considered a black radiant panel and the radiative flux is expressed with Stefan–Boltzmann modelling:

$$\phi_b = BT^4 h \quad (10)$$

where B, T and h are the Stefan–Boltzmann constant, mean flame temperature and fuel height respectively. Mean flame temperature is obtained from the thermal balance in the flame body (see Appendix B for details).

Energy losses from the top of the preheating zone (BD) are proportional to extinction depth δ (length of the flame base for which the vertical flame body radiation is close to zero) and inversely proportional to the height of the radiant panel, h. The expression of the scaling factor a_b is given by:

$$a_b = \min\left(2\frac{h}{\delta}, 1\right) \quad (11)$$

The expression for the extinction depth is (see details in Appendix B):

$$\delta = \frac{2\pi}{s\beta} \quad (12)$$

where s and β are surface area to volume ratio of fine fuel and packing ratio respectively.

Finally, if S ($S = s\beta h$) is the total fuel surface area per horizontal area unit of fuel bed and denotes the double of the leaf area index (LAI), and if ρ_v denotes the fuel density,

$$R_b = \min\left(2\frac{S}{2\pi}, 1\right)\frac{BT^4}{\beta \rho_v q} \quad (13)$$

Note that Balbi *et al.* (2009) used a model parameter to express the scaling factor a_b. Thus, Eqn 11 (and therefore Eqn 13) is a clear improvement with the removal of this model parameter.

Flame radiative heat flux

The flame body (above the vegetation stratum) is assumed to be a grey radiant panel with emissivity ε; the expression for the radiative flux is the following (see Fig. 1):

$$\phi_r = \varepsilon BT^4 \int_D^B \left(\frac{1}{\pi}\int_{ABI} \frac{\cos\varphi_1 \cos\varphi_2}{d^2} d\sum\right) dx \quad (14)$$

where d denotes the distance between a point M (whose abscissa is x), belonging to the segment $[BD]$ and a point P from the fire front panel, and φ_1 and φ_2 denote the angles between the straight line (MP) and the normals to the fire front and to the ground respectively.

After some calculations (detailed in Appendix C), Eqn 14 leads to the flame radiative contribution:

$$R_r = AR\frac{1 + \sin\gamma - \cos\gamma}{1 + \frac{R\cos\gamma}{s r_{00}}} \quad (15)$$

Table 1. Nomenclature of model variables and fuel bed characteristics

Latin symbols		
A	Radiation coefficient	
a	Scaling factor	
B	Stefan–Boltzmann constant (W m^{-2} K^{-4})	5.6×10^{-8}
c	Char fraction	
C_{pw}	Specific heat of water (J kg^{-1} K^{-1})	4180
C_p	Specific heat of fuel (J kg^{-1} K^{-1})	
C_{pa}	Specific heat of air (J kg^{-1} K^{-1})	1150
g	Acceleration due to gravity (m s^{-2})	9.81
h	Fuel bed depth (m)	
H	Flame height (m)	
k	Catchpole *et al.* (1998) moisture damping coefficient	
K	Law for drag forces	
K_1	Drag coefficient (s m^{-1})	130
l	Flame length (m)	
L	Flame depth (m)	
m	Fuel moisture content	
p	Proportionality coefficient	
q	Ignition energy (J kg^{-1})	
r_{00}	Model coefficient	2.5×10^{-5}
R	Rate of fire spread (m s^{-1})	
R_b	Contribution of radiation of burning fuel bed to ROS (m s^{-1})	
R_c	Contribution of convection to ROS (m s^{-1})	
R_r	Contribution of flame radiation to ROS (m s^{-1})	
s	Surface area-to-volume ratio of fine fuel (m^{-1})	
S	Leaf area per square metre (m^2 m^{-2})	
s_t	Air–pyrolysis gas mass ratio in the flame body	17
S_f	Surface flame area (m^2)	
T	Mean flame temperature (K)	
T_a	Ambient temperature (K)	300
T_i	Ignition temperature (K)	600
T_w	Mean water temperature (K)	
T_v	Mean fuel temperature (K)	
T_{vap}	Vaporisation temperature (K)	373
U	Sum of normal (to the fire front) component of the natural wind velocity and fire-generated inflow coming from the burnt area (m s^{-1})	
U'	Velocity of the fire-generated inflow coming from the unburnt area (m s^{-1})	
$U(x)$	Air stream velocity within the burning fuel bed (m s^{-1})	
u_c	Upward gas velocity at the top of the flame base (m s^{-1})	
u_0	Upward gas velocity at flame body mid-height on flat terrain (m s^{-1})	
u	Upward gas velocity at flame body mid-height on sloping terrain (m s^{-1})	
V_f	Volume flame (m^3)	
x	Abscissa (defined in Fig. 2)	
Greek symbols		
α	Terrain slope angle (°)	
β	Packing ratio	
δ	Optical depth	
γ	Flame tilt angle (°)	
γ_c	Angle defined in Fig. 1 (°)	
ε	Flame emissivity	
χ	Radiative fraction	
χ_0	Radiative factor	0.3
ΔH	Heat of combustion of the pyrolysis gases (J kg^{-1})	1.74×10^7
Δh	Heat of latent evaporation (J kg^{-1})	2.3×10^6
ρ_v	Fuel particle density (kg m^{-3})	
$\dot{\sigma}$	Derivative of the dead fuel load over time	
σ	Dead fuel load (kg m^{-2})	
σ_v	Total fuel load (dead fuel load and fuel water load; kg m^{-2})	
σ_w	Fuel water load (kg m^{-2})	
θ	View angle of the flame (°)	
ϕ	Heat flux per unit length (W m^{-1})	
φ_1,φ_2	Angles between straight line (MP in Fig. 1) and the normal to the fire front and to the ground, respectively.	
τ_0	Flame residence time parameter (s m^{-1})	75 591
τ	Flame residence time (s)	
Subscripts		
a	Related to air	
b	Related to flame base	
c	Related to convective warming	
cc	Related to convective cooling	
r	Related to flame body	
u	Related to an effective variable	
w	Related to fuel water	
Abbreviations		
CFD	Computational fluid dynamics	
FB	Fractional bias	
FMC	Fuel moisture content	
LAD	Leaf area density	
LAI	Leaf area index	
NMSE	Normalised mean square error	
ROS	Rate of spread	

where r_{00} is a model coefficient. A is a radiative factor defined by:

$$A = a_r \frac{\chi_0 \Delta H}{4q} \tag{16}$$

where ΔH and χ_0 are the heat of combustion of the pyrolysis gases and a radiative factor respectively. The scaling factor a_r is equal to 1 if the extinction depth is smaller than the fuel thickness (which means that the unburnt fuel absorbs all the radiative energy) and depends on the leaf area otherwise:

$$a_r = \min\left(\frac{S}{2\pi}, 1\right) \tag{17}$$

Eqns 13 and 15 are the core of the radiative-only model developed by Balbi *et al.* (2007, 2009) and improved by Balbi *et al.* (2010). This radiative-only model provided good results for fire spread experiments across litter (Weise *et al.* 2016) but convective effects were neglected and some model parameters varied from one experiment to another. These shortcomings vanish in the current proposed model.

Convective heat flux

The flame that contacts the unburnt fuel (flame inside the rectangle BCC_0B_0 in Fig. 1) is supplied by an amount of pyrolysis gases that is proportional to the area delimited by streamline 1 in the flame base (points EBB_0A_0 in Fig. 1). This area is

approximated by the surface of the triangle B_0BF, which is defined by the angle γ_c:

$$\tan\,\gamma_c = \tan\,\alpha + \frac{U(L)}{u_c} \tag{18}$$

$U(L)$ and u_c are horizontal wind speed at point B and upward gas velocity at the top of the flame base respectively. Decreasing wind speed along the flame base was observed by Anderson *et al.* (2010) and is expressed (Chatelon *et al.* 2017) as follows (assuming a local equilibrium between inertia and drag forces):

$$U(x) = U\,exp\,(-Kx) \tag{19}$$

where K models the drag forces and x represents the abscissa defined as in Fig. 2. It is assumed that K depends on fuel porosity as follows:

$$K = K_1^* s\beta^{\frac{1}{2}} \tag{20}$$

where K_1* is a drag coefficient. After some calculus (see details in Appendix D), the final profile for wind speed at the burning fuel–unburnt fuel interface is the following:

$$U(L) = U\,exp\left(-K_1\beta^{\frac{1}{2}}R\right) \tag{21}$$

where K_1 is a drag coefficient (see Appendix D).

Upward gas velocity u_c is computed at the top of the flame base and is assumed to depend on vertical gas velocity u_0, which is computed at flame mid-height (Eqn B8 in Appendix B). Thus, the expression for u_c is obtained by taking into account changes in the outflow (sections vary from L to $L/2$) and in the height (which varies from $h + H/2$ to h):

$$u_c = \frac{h}{h+\frac{H}{2}}\frac{u_0}{2} \tag{22}$$

The expression for the flame height H is given by (Balbi *et al.* 2009):

$$H = \frac{u_0^2}{g\left(\frac{T}{T_a}-1\right)} \tag{23}$$

where g is gravity acceleration.

As the pyrolysis gas flow coming from the triangular fuel area BB_0F is equal to the product of the flame base flow and the triangle/flame base surface ratio, convective heat flux is expressed as:

$$\phi_c = \Delta HL\,\dot{\sigma}\frac{Area(BB_0F)}{Area(ABB_0A_0)} \tag{24}$$

where σ is the derivative of the dead fuel load over time.

Eqn 24 finally gives (see Appendix E for calculus details):

$$\phi_c = \frac{\Delta H}{2\tau_0}\sigma s\,\min(h,\delta)\tan\gamma_c \tag{25}$$

where τ_0 denotes a flame residence time parameter.

The scaling factor a_c for this convective flux depends on energy losses from the upper and lower parts of the vegetation stratum. At laboratory scale, the floor is assumed to be adiabatic and then no heat losses are possible at the ground interface. Energy losses at the top of the vegetation stratum are given by the ratio between the surface of the flame that is in contact with the unburnt fuel and the total flame surface (which is approximately the ratio between the area of rectangle BCC_0B_0 and the sum of the areas of this rectangle and triangle BCI). So the modelling for the scaling factor a_c is the following (with terms defined in Fig. 1):

$$a_c = \frac{h\overline{BC}}{h\overline{BC}+\frac{1}{2}h\overline{BC}} = \frac{h}{h+\frac{H}{2}} \tag{26}$$

Finally, using the expression of flame residence time given by Andrews (1986) that is inversely proportional to the surface area-to-volume ratio, combining Eqn 7 and Eqn 26 yields (see Appendix E for details):

$$R_c = \frac{\Delta H}{q\tau_0}s\,\min\left(h,\frac{2\pi}{s\beta}\right)\left(\frac{h}{2h+H}\tan\alpha + \frac{U\,exp\left(-K_1\beta^{\frac{1}{2}}R\right)}{u_0}\right) \tag{27}$$

Main equation of the model

The ROS is the sum of the three contributions previously given in Eqns 13, 15, 27:

$$R = \min\left(\frac{S}{\pi},1\right)\frac{BT^4}{\beta\rho_v q} + \frac{s\,\Delta H}{q\,\tau_0}\min\left(h,\frac{2\pi}{s\,\beta}\right)\left(\frac{h}{2h+H}\tan\alpha + \frac{U\,exp\left(-K_1\beta^{\frac{1}{2}}R\right)}{u_0}\right) + AR\frac{1+\sin\gamma-\cos\gamma}{1+\frac{R\cos\gamma}{s\,r_{00}}} \tag{28}$$

Eqn 28 is a non-linear algebraic equation that is solved directly thanks to a fixed-point method (iterative method with R_b as initialisation value).

Note that the model includes three universal parameters: a drag coefficient K_1, a stoichiometric coefficient s_t (ratio between fresh air and pyrolysis gases), and a model coefficient r_{00} (in the law for the ratio between radiative fraction and flame thickness).

The value of these three fitted parameters, $K_1 = 130$, $s_t = 17$ (Chatelon *et al.* 2017) and $r_{00} = 2.5 \times 10^{-5}$ (Balbi *et al.* 2010) does not change from one experiment to another. The only parameters that change between two experiments are fuel characteristics, terrain slope angle and wind speed. So the proposed model is fully predictive, without model parameters that vary between two experiments.

Numerical results

At laboratory scale, experimental conditions can be fully controlled with the guarantee of a high level of repeatability of experimental results. Thus, the assessment of results obtained

Table 2. Numerical simulations performed in order to visualise the main tendencies of the predicted rate of spread (ROS) versus wind and fuel moisture content (FMC)

Numerical simulations	Wind velocity U (m s^{-1})	Main fuel characteristics				
		Surface area to volume ratio s (m^{-1})	Fuel height h (m)	FMC m (%)	Fuel density ρ_v (kg m^{-3})	Fuel load σ (kg m^{-2})
ROS *v.* wind	0 to 10 (step = 0.4)	6000	0.1	10	500	0.05; 0.3; 0.8
ROS *v.* FMC	0.2; 8	6000	0.1	5 to 90 (step = 5)	500	0.09

with the proposed model at this scale is an essential preliminary step before extending its use to a larger scale. In order to quantify the error between predicted and measured values, three statistics tools are used: an estimate of overall deviation (normalised mean square error, NMSE), a measure of the linear correlation (Pearson correlation coefficient) and the fractional bias (FB), which estimates model underprediction or overprediction.

The value of the drag coefficient K_1 is determined as the best value that fits the Nelson and Adkins (1986) pine needle fire experiments. Nelson and Adkins carried out a set of laboratory experiments over a bed of fresh slash pine needles (*Pinus elliottii*) with two different fuel loads (0.54 and 1.055 kg m^{-2}). Very good agreement between predicted and observed ROS with a very small deviation (NMSE = 5.43%) and a strong correlation ($r = 0.95$) are obtained for $K_1 = 130$. So, as K_1 is assumed to be a universal coefficient, its value will no longer change, whatever laboratory experiments the proposed model is applied to.

Before applying the proposed model to laboratory experiments, several numerical simulations were performed in order to observe the main tendencies of the predicted ROS in relation to wind and fuel moisture content (FMC).

Numerical simulations

The theoretical trend of ROS depends on the value of the radiative coefficient A (Eqn 16). In order to obtain the trend of ROS with wind velocity, several numerical tests were run. Wind velocity ranged from 0 to 10 m s^{-1} (with a 0.4-m s^{-1} step) and three different values of fuel load were considered, which led to three different values of coefficient A. Other fuel characteristics did not change from one simulation to another (data and results respectively given in Table 2 and Fig. 3). Fig. 3 shows three different curves for ROS:

- When coefficient A is much lower than 1 ($A = 0.15$ with $\sigma = 0.05$ kg m^{-2}), a fast increase at the start and then a slowing in ROS increase characterise the ROS trend. In this case, flame radiation is practically negligible and the propagation is driven by flame base radiation and convection.
- When coefficient A is close to 1 ($A = 1.01$ with $\sigma = 0.3$ kg m^{-2}), a practically linear ROS trend is observed.
- When coefficient A is greater than 1 ($A = 1.51$ with $\sigma = 0.8$ kg m^{-2}), ROS slowly increases with wind velocity at the start and then accelerates. In this case, fire spread is basically due to flame radiation and convection. Flame base radiation does not play a major role.

Note that these three different ROS curves are similar to the ones observed by Rothermel and Anderson (1966).

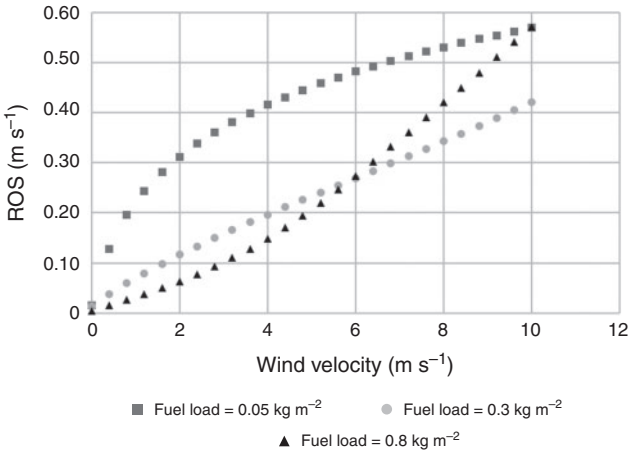

Fig. 3. Numerical simulations of the rate of spread (ROS) against wind velocity for three different values of fuel load.

The effect of FMC on the ROS has been widely reported in the literature (Marsden-Smedley *et al.* 2001; Morvan 2013; Rossa *et al.* 2016; Weise *et al.* 2016; Rossa 2017). Usually, the effect of FMC is summarised using the ratio ROS/ROS(0%) where ROS(0%) is the theoretical value of ROS observed when the FMC is zero. The trend of ROS with FMC may be a good marker for the relevance of a propagation model. Numerical simulations of the model *v.* FMC were carried out for two different values of wind velocity ($U = 0.2$, 8 m s^{-1}). Fuel characteristics are presented in Table 2. Fig. 4 shows the decrease of ROS with FMC for the two wind velocities, but this decrease is faster for the lower wind velocity, which agrees with the results found by Morvan (2013). ROS for the larger wind velocity seems to be much closer to a linear trend.

Testing the proposed model

The proposed model was applied to a large set of laboratory fires carried out by Catchpole *et al.* (1998). Catchpole *et al.* (1998) conducted 357 laboratory fires over a wide range of particle sizes, fuel bed depths, packing ratios, moisture contents and wind velocities. Two different fuels – *Pinus ponderosa* and *Populus tranulos* (poplar excelsior) – were used. *Pinus ponderosa* fire experiments were categorised as well-ordered and vertically oriented fuel beds (heartwood sticks) and continuous fuel beds (needles). As Chatelon *et al.* (2017) successfully tested the convective model against heartwood stick fires with a small NMSE (2.11%), a slight overestimation (FB = 0.05) and good correlation

($r = 0.96$), the proposed radiative–convective model was then tested against the 334 experimental fires with continuous fuel beds. Note that the specific heat of vegetation C_p is calculated using Eqn 9 and the approximation for the heat of pre-ignition used by Catchpole *et al.* (1998). Values of 2370 and 2030 J kg^{-1} K^{-1} were found for excelsior and pine needles respectively.

The scatter diagram shown in Fig. 5 indicates that the predicted ROS matches experimental ROS with a small mean deviation under the 10% level (NMSE = 7.25%). The line of perfect agreement is represented by the plain line. The bias of the proposed model is slightly negative (FB = –0.06), which means that the model barely underestimates the measured ROS. The Pearson correlation coefficient is close to 1 ($r = 0.94$), which indicates that the correlation between predictions of the radiative–convective Balbi model and experimental ROS is satisfactory. Fig. 6 presents scatter diagrams for each type of fuel bed.

Fig. 7 and Table 3 display error results for each fuel type (ponderosa pine needles, regular excelsior and coarse excelsior). Note that the slight underestimation of the measured ROS is not a global trend of the model because Table 3 shows that although the model underestimates experimental ROS in excelsior fuel beds, it overestimates ROS in pine needle fuel beds.

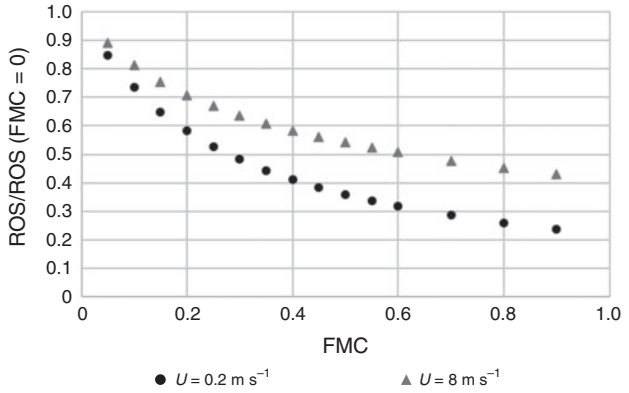

Fig. 4. Relative decay of the rate of spread (ROS; ROS/ROS(0%)) *v.* fuel moisture content (FMC).

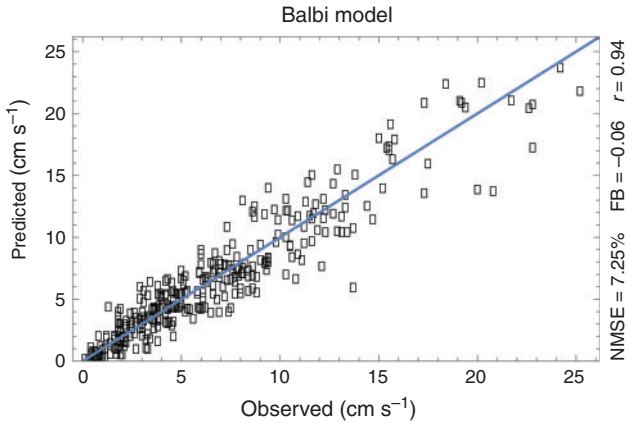

Fig. 5. Predicted rate of spread (ROS) given by the proposed model *v.* observed rate of spread in the set of experiments of Catchpole *et al.* (1998).

In order to obtain the values of ROS *v.* FMC, a data subset with the same fuel characteristics and wind velocity was chosen among the large set of experiments performed by Catchpole *et al.* (1998). Fig. 8 shows the decrease of ROS *v.* FMC for this data subset ($U = 1.8$ m s^{-1}, $s = 7596$ m^{-1}, $\beta = 0.02$, $h = 0.08$ m, $\sigma = 0.6$ kg m^{-2}, $\rho_v = 398$ kg m^{-3}).

Note that the proposed model is a simplified physical model for surface fire propagation, and thus computational time is very

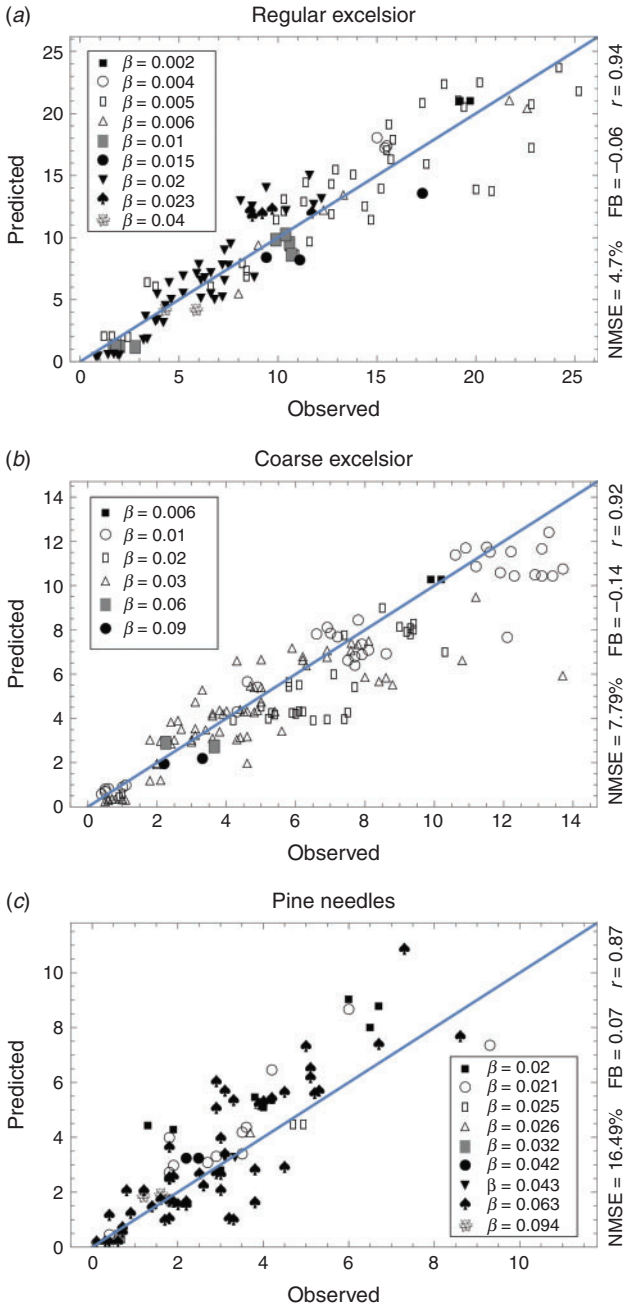

Fig. 6. Predicted rate of spread (ROS) given by the proposed model *v.* observed rate of spread in the set of experiments of Catchpole *et al.* (1998) for different values of packing ratio where fuel bed is regular excelsior (*a*); coarse excelsior (*b*); and *Pinus ponderosa* needles (*c*).

short (less than 1 s to simulate the whole set of laboratory fires on a MacBook Pro laptop with an i7 processor).

Model comparison

Catchpole *et al.* (1998) built an empirical model for ROS that fits their data very well. This simple model is based on energy conservation and experimental laboratory fires, and depends on wind velocity and fuel bed properties. The moisture damping coefficient (denoted k) is the only fitted parameter, and in the present notation, the model equation is the following:

$$R = \frac{(495 + 1934U^{0.91})exp\left(-\frac{347}{s}\right)}{\rho_v\sqrt{\beta}\left(Q_p + m\Delta h\right)}exp\left(-km\right) \qquad (29)$$

where Q_p is the heat of pyrolysis of a unit mass of dry fuel.

Catchpole *et al.* (1998) suggested that the moisture damping coefficient might depend on packing ratio, fuel particle size, or both, and a different value for each fuel type is reported ($k = 0$ for regular excelsior, 2.03 for coarse excelsior and 4.05 for pine needles). The simple Catchpole model fits the data better than the proposed model in terms of error and correlation (NMSE = 4.21%, FB = 0 and $r = 0.97$), which makes sense because it was specifically developed from these datasets. Detailed results and a scatter diagram are presented in Table 3 and Fig. 9 respectively.

The difference between predicted ROS given by the proposed model and the Catchpole model is small (~3% error) and one important aspect of the proposed model is the absence of model parameters that vary from one experiment to another, which makes the model fully predictive. Indeed, the Catchpole model needs a different value of moisture damping coefficient (which varies from approximately 0 to 4) not only for each fuel but for each fuel type. This value is determined according to measured ROS. Thus, the Catchpole model is not a predictive model, in contrast to the proposed model.

The value of the moisture damping coefficient that best fits the whole set of experiments is 2 ($k = 2$). In this case, the

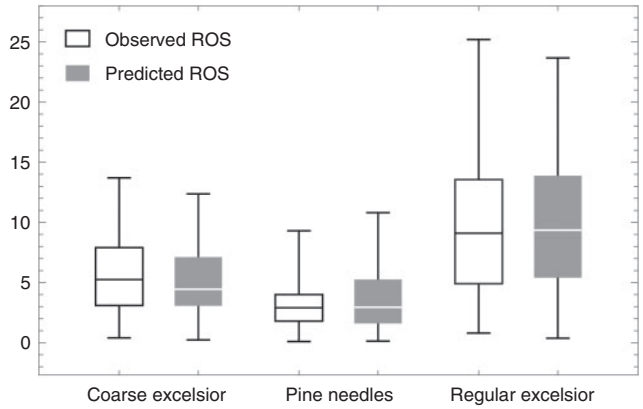

Fig. 7. Box and whisker plot of the predicted rate of spread (ROS) given by the proposed model *v.* observed rate of spread in the set of experiments of Catchpole *et al.* (1998) for each fuel type.

Table 3. Comparison of normalised mean square error (NMSE), fractional bias (FB) and Pearson's correlation coefficient (r) obtained by the radiative-convective Balbi model and by the Catchpole simple model for each fuel type when simulating the experiments carried out by Catchpole *et al.* (1998)

Fuel type	No. of fires	Proposed model			Catchpole *et al.* model		
		NMSE (%)	FB	r	NMSE (%)	FB	r
Pinus ponderosa needles	85	16.49	0.07	0.87	10.81	0.01	0.87
Coarse excelsior	141	7.79	−0.14	0.92	4.76	−0.01	0.94
Regular excelsior	108	4.70	−0.06	0.94	2.57	0	0.97
All fires	334	7.25	−0.06	0.94	4.21	0	0.97

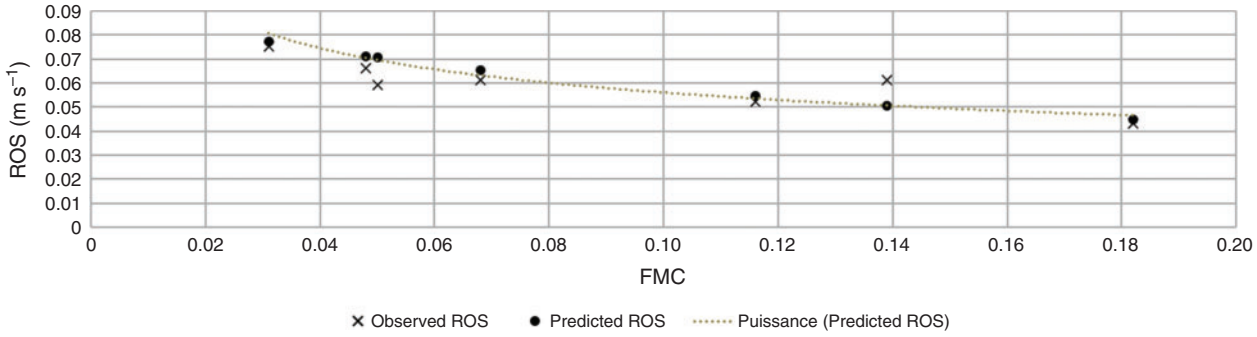

Fig. 8. Predicted rate of spread (ROS) *v.* fuel moisture content (FMC) in a data subset of the set of experiments of Catchpole *et al.* (1998). Wind velocity, surface area-to-volume ratio, packing ratio, fuel height, fuel load and fuel density are the same for each fire in this data subset ($U = 1.8$ m s^{-1}, $s = 7596$ m^{-1}, $\beta = 0.02$, $h = 0.08$ m, $\sigma = 0.6$ kg m^{-2}, $\rho_v = 398$ kg m^{-3}).

simple Catchpole model provides an error of ~6.5% (NMSE = 6.52%) with very good correlation ($r = 0.95$) and then the model is predictive. But Chatelon *et al.* (2017) showed that the Catchpole model gave poor results when applied to other experiments using sticks, which makes sense because the values of the damping moisture coefficient were fitted to the Catchpole dataset.

Nevertheless, Table 3 shows that both models show the same tendency in relation to error. Indeed, the NMSE for the pine needle experimental fires is largest for both the Catchpole model and proposed model and the smallest NMSE is obtained for the regular excelsior fires.

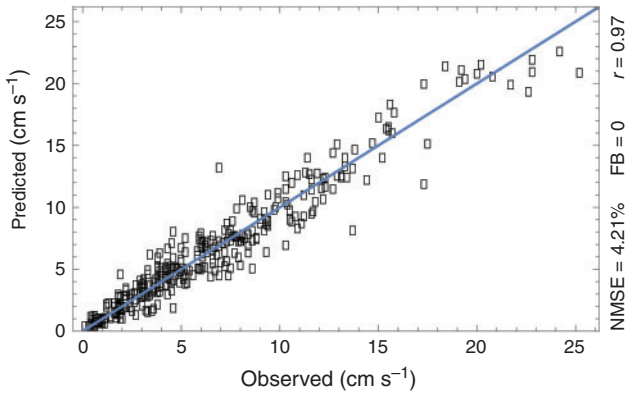

Fig. 9. Predicted rate of spread (ROS) given by the Catchpole simple model *v*. observed rate of spread in the Catchpole *et al.* (1998) set of experiments.

The proposed simplified physical model was also compared with a detailed physical model integrated into the FIRESTAR CFD software (Morvan *et al.* 2009, 2018; Frangieh *et al.* 2018).

FIRESTAR is a 2D-3D multiphase CFD model specifically dedicated to simulating the behaviour of wildfires at a local scale (less than 500–1000 m). The numerical code is structured into two major parts: the first one to follow the evolution of the state of the vegetation layer, the second one to calculate the fire front and the evolution of the surrounding atmosphere. Each part has its own set of equations solved in its own mesh. Coupling between the vegetation and gas phase is performed, by modelling this solid phase as a sparse porous medium (the solid fraction in a vegetation layer does not exceed few percent in a fuel bed), structured as a collection of solid fuel particles representing the leaves, twigs, branches, trunk of each plant species. Then an averaging process is applied to the balance equation (mass, momentum, energy, …), similarly to a homogenisation step. This preliminary treatment results in introducing a set of additional terms representing interactions between solid and gaseous phases. As an example, in the momentum equation, the presence of the vegetation is taken into account using a volumetric distribution of drag forces proportional to the square of the velocity with a drag coefficient defined from the leaf area density (LAD).

The model includes the calculation of the evolution of temperature, fuel volume fraction and composition (moisture

Table 4. Comparison between predicted rate of spread (ROS) obtained with FireStar2D and Balbi Model and observed ROS for a sample of laboratory fires performed by Catchpole *et al.* (1998)

The surface area-to-volume ratio and fuel density are respectively: 5710 m^{-1} and 510 kg m^{-3} for the pine needle fires; 3092 m^{-1} and 398 kg m^{-3} for the coarse excelsior fires; and 7596 m^{-1} and 398 kg m^{-3} for the regular excelsior fires

Fuel type	Packing ratio β	FMC m	Fuel bed depth (cm)	Wind speed U (m s^{-1})	Observed ROS (cm s^{-1})	FireStar2D ROS (cm s^{-1})	Balbi ROS (cm s^{-1})
Pine needles	0.02	0.059	7.6	2.68	6	5.4	8.9
	0.021	0.065	7.6	0	0.4	1.56	0.41
	0.021	0.265	7.6	2.68	3.6	2.24	4.33
	0.021	0.123	7.6	1.34	2.7	2.51	3
	0.021	0.246	7.6	1.79	1.9	2.01	2.9
	0.021	0.093	7.6	1.34	3.5	4.78	3.3
	0.063	0.066	7.6	1.34	1.8	3.75	1.61
	0.063	0.056	7.6	2.68	2.9	3.77	5.9
Coarse excelsior	0.02	0.036	7.6	1.34	5	12.03	4.5
	0.02	0.08	7.6	1.34	6.9	10.15	3.9
	0.02	0.062	7.6	1.79	5.8	8.52	5.4
	0.03	0.037	7.6	0	0.7	1.67	0.36
	0.03	0.058	7.6	1.34	4.6	6.06	3.15
	0.03	0.239	7.6	1.34	2	3.69	1.95
Regular excelsior	0.005	0.042	7.6	0.45	3.8	0	6
	0.005	0.035	7.6	1.34	11.3	12.2	12.8
	0.005	0.08	7.6	1.79	15.2	12.69	13.9
	0.005	0.039	7.6	2.68	22.8	12.73	20.7
	0.02	0.034	7.6	0	1.7	1.71	0.54
	0.02	0.027	7.6	1.34	6.6	7	5.41
	0.02	0.19	7.6	1.34	3.8	2.76	3.21
	0.02	0.05	7.6	1.79	5.9	6.19	7

content, dry fuel, charcoal, ash) of each solid fuel family constituting the vegetation stratum.

All the main physical phenomena (turbulence, heat transfers by convection and radiation, combustion, …) contributing to the behaviour of the fire front were taken into account in the CFD model in the gaseous phase.

Morvan (2011) simulated a sample of fires among the large dataset given by Catchpole *et al.* (1998) with FIRESTAR2D. All data and results are given in Table 4. A comparison between numerical results obtained with FIRESTAR2D and the proposed model is made in Fig. 10. Table 5 shows that for the selected group of fires, the proposed model has better agreement than FIRESTAR2D, with a smaller NMSE (7.21 *v.* 31.09%) and better correlation ($r = 0.95$ *v.* 0.79). FIRESTAR2D provides good numerical results for pine needles fires but poor results for excelsior fires, whereas the proposed model is far more accurate for excelsior fires.

Morvan *et al.* (2018) provided a simulation on another sample of fires using the 3D version of FIRESTAR. Data and numerical ROS are provided in Table 6 and Fig. 11 presents the scatter diagram of Balbi ROS/FIRESTAR3D ROS *v.* observed ROS. The error in ROS given by the proposed model and FIRESTAR3D are both small (NMSE = 1.76 and 8.00% respectively). If both models neither overestimate nor underestimate observed ROS with a bias close to zero (FB = 0.00 and 0.02 respectively), the proposed model provides a better correlation ($r = 0.91$) than FIRESTAR3D ($r = 0.83$).

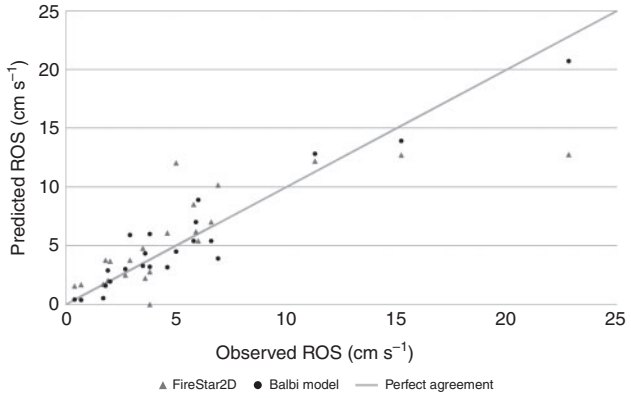

Fig. 10. Predicted rate of spread (ROS) given by the proposed model and FIRESTAR2D *v.* observed rate of spread in a sample of fire experiments performed by Catchpole *et al.* (1998).

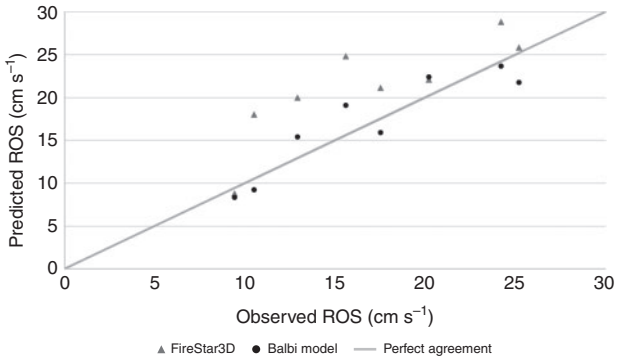

Fig. 11. Predicted rate of spread (ROS) given by the proposed model and FIRESTAR3D *v.* observed rate of spread in a sample of fire experiments performed by Catchpole *et al.* (1998).

Table 5. Comparison of normalised mean square error (NMSE), fractional bias (FB) and Pearson's correlation coefficient (r) obtained by the radiative-convective Balbi model and the CFD software FireStar2D when simulating a sample of fires carried out by Catchpole *et al.* (1998)

Fuel type	No. of fires	Proposed model			FireStar2D		
		NMSE (%)	FB	r	NMSE (%)	FB	r
Pinus ponderosa needles	8	19.35	0.03	0.92	13.21	0.01	0.75
Coarse excelsior	6	8.60	−0.04	0.87	41.77	0.08	0.87
Regular excelsior	8	3.64	0	0.98	25.29	−0.03	0.87
All fires	22	7.21	0	0.95	31.09	0	0.79

Table 6. Comparison between predicted rate of spread (ROS) obtained with FireStar3D and Balbi Model and observed ROS for a sample of regular excelsior laboratory fires performed by Catchpole *et al.* (1998)

Fuel height, surface area-to-volume ratio and fuel density are respectively equal to 7.6 cm, 7596 m^{-1} and 398 kg m^{-3} for all the selected fires

Fuel height (cm)	Packing ratio β	FMC m	Wind speed U (m s^{-1})	Observed ROS (cm s^{-1})	FireStar3D ROS (cm s^{-1})	Balbi ROS (cm s^{-1})
20.3	0.005	0.055	2.68	25.2	25.8	21.78
	0.005	0.052	0.89	10.5	18	9.25
	0.005	0.054	1.79	12.9	20	15.4
	0.005	0.101	2.68	15.6	24.8	19.09
	0.005	0.181	2.68	17.5	21.1	15.9
	0.005	0.03	2.68	24.2	28.8	23.66
	0.015	0.049	1.79	9.4	8.8	8.33
15.2	0.005	0.045	2.68	20.2	22.1	22.4

Conclusion

This work deals with a simplified physical model of surface fire propagation that is a combination of a radiative-only model (Balbi *et al.* 2010) and a convective model (Chatelon *et al.* 2017). The ROS is the solution of a non-linear algebraic equation that depends on wind velocity, terrain slope angle and fuel characteristics (moisture content, thickness, packing ratio, surface-area-to-volume ratio, etc.). The proposed model takes into account four sources of heat transfer: flame base radiation, flame radiation, convective cooling and convective warming. The convective warming effects are the result of the flow of hot gases inside the flame base. Indeed, the flow of hot gases, subject to upward gas velocity and wind velocity, creates a contact flame that preheats and ignites the unburnt fuel.

The model includes three universal parameters: a parameter that expresses the effect of flame thickness on the radiative fraction, a stoichiometric coefficient that represents the air/pyrolysis gases ratio in the flame body and a drag coefficient. The value of these three coefficients never changes regardless of the fire experiments. So, in contrast to the radiative model developed by Balbi *et al.* (2010), the proposed model has no parameter that varies from one experiment to another, and thus is fully predictive.

Moreover, the proposed model is much faster than real time owing to its characteristic of being a simplified physical model and thus could be used by firefighters or fire management personnel.

The proposed model was tested against more than 300 experimental fires conducted by Catchpole *et al.* (1998), with a good correlation between predicted and observed ROS and an error below 8%, which expresses a satisfactory accuracy.

The use of the proposed model can be easily extended to larger scales with a few changes. For instance, the ground interface on the field is no longer assumed to be adiabatic, so a slight change in the scaling factor a_c (Eqn 26) is necessary. Moreover, the drag coefficient K_1 may have a lower value at field scale because of the composition of the vegetation stratum. However, a highly significant feature of this approach is that the model is not dependent on scale issues and requires low computational time.

Conflicts of interest

The authors declare they have no conflicts of interest.

Acknowledgements

The present work was supported in part by the French Ministry of Research, the Corsican Region and the CNRS (Centre National de la Recherche Scientifique), under grant CPER 2007–2013. The authors also wish to thank Mr Pierre-Régis Gonsolin for his help with English reviewing.

References

Albini FA (1982) Response of free-burning fires to non-steady wind. *Combustion Science and Technology* **29**, 225–241. doi:10.1080/00102208208923599

Albini FA (1985) A model for fire spread in wildland fuels by radiation. *Combustion Science and Technology* **42**, 229–258. doi:10.1080/00102208508960381

Albini FA (1986) Wildland fire spread by radiation – a model including fuel cooling by natural convection. *Combustion Science and Technology* **45**, 101–113. doi:10.1080/00102208608923844

Anderson WR, Catchpole EA, Butler BW (2010) Convective heat transfer in fire spread through fine fuel beds. *International Journal of Wildland Fire* **19**, 284–298. doi:10.1071/WF09021

Andrews PL (1986) BEHAVE: Fire behavior prediction and fuel modeling system – BURN subsystem, Part 1. USDA Forest Service, Intermountain Research Station, General Technical Report INT-194. (Ogden, UT, USA)

Balbi J-H, Rossi J-L, Marcelli T, Santoni P-A (2007) A 3D physical real-time model of surface fires across fuel beds. *Combustion Science and Technology* **179**, 2511–2537. doi:10.1080/00102200701484449

Balbi J-H, Morandini F, Silvani X, Filippi JB, Rinieri F (2009) A physical model for wildland fires. *Combustion and Flame* **156**, 2217–2230. doi:10.1016/J.COMBUSTFLAME.2009.07.010

Balbi J-H, Rossi J-L, Marcelli T, Chatelon F-J (2010) Physical modeling of surface fire under non-parallel wind and slope conditions. *Combustion Science and Technology* **182**, 922–939. doi:10.1080/00102200903485178

Balbi J-H, Chatelon FJ, Rossi JL, Simeoni A, Viegas DX, Rossa C (2014) Modelling of eruptive fire occurrence and behaviour. *Journal of Environmental Science and Engineering B* **3**, 115–132.

Catchpole WR, Catchpole EA, Butler BW, Rothermel RC, Morris GA, Latham DJ (1998) Rate of spread of free-burning fires in woody fuels in a wind tunnel. *Combustion Science and Technology* **131**, 1–37. doi:10.1080/00102209808935753

Catchpole WR, Catchpole EA, Tate AG, Butler B, Rothermel RC (2002) A model for the steady spread of fire through a homogeneous fuel bed. In 'Proceedings of 4th International Conference on Forest Fire Research, 2002 Wildland Fire Safety Summit, 18–23 November 2002, Luso–Coimbra, Portugal.' (Ed. DX Viegas) (Millpress: Rotherdam)

Chatelon FJ, Balbi JH, Morvan D, Rossi JL, Marcelli T (2017) A convective model for laboratory fires with well-ordered vertically oriented fuel beds. *Fire Safety Journal* **90**, 54–61. doi:10.1016/J.FIRESAF.2017.04.022

Chatelon F-J, Balbi JH, Rossi J-L, Marcelli T (2018) Upslope fire and eruptive fire. In 'Fire contin. conf. – prep. futur. wildl. fire (Fire Behav. Sci. Sess.', Missoula, MT)

Cheney NP, Gould JS, Catchpole WR (1998) Prediction of fire spread in grasslands. *International Journal of Wildland Fire* **8**, 1–13. doi:10.1071/WF9980001

De Mestre NJ, Catchpole EA, Anderson DH, Rothermel RC (1989) Uniform propagation of a planar fire front without wind. *Combustion Science and Technology* **65**, 231–244. doi:10.1080/00102208908924051

Dold JW, Zinoviev A (2009) Fire eruption through intensity and spread rate interaction mediated by flow attachment. *Combustion Theory and Modelling* **13**, 763–793. doi:10.1080/13647830902977570

El Houssami M, Thomas JC, Lamorlette A, Morvan D, Chaos M, Hadden R, Simeoni A (2016) Experimental and numerical studies characterizing the burning dynamics of wildland fuels. *Combustion and Flame* **168**, 113–126. doi:10.1016/J.COMBUSTFLAME.2016.04.004

Finney MA, Cohen JD, Grenfell IC, Yedinak KM (2006) Experiments on fire spread in discontinuous fuelbeds. In 'Proceedings of the V international conference on. Forest fire research', November 27–30, Coimbra, Portugal. (Ed. DX Viegas)

Finney MA, Cohen JD, Forthofer JM, McAllister SS, Gollner MJ, Gorham DJ, Saito K, Akafuah NK, Adam BA, English JD (2015) Role of buoyant flame dynamics in wildfire spread. *Proceedings of the National Academy of Sciences of the United States of America* **112**, 9833–9838. doi:10.1073/PNAS.1504498112

Frangieh N, Morvan D, Meradji S, Accary G, Bessonov O (2018) Numerical simulation of grassland fires behavior using an implicit physical multiphase model. *Fire Safety Journal* **102**, 37–47. doi:10.1016/J.FIRESAF.2018.06.004

Grishin AM (1997) 'Mathematical modeling of forest fires and new methods of fighting them.' (Ed. FA Albini) (Publishing House of the Tomsk University: Tomsk, Russia).

Grumstrup TP, McAllister SS, Finney MA (2017) Qualitative flow visualization of flame attachment on slopes. In 'U. S. National Combustion Meeting Organized by the Eastern States Section of the Combustion Institute; April 23–26, 2017; College Park, MD.' pp. 1–6. (The Combustion Institute: Pittsburgh, PA) Available at https://www.fs.usda.gov/treesearch/pubs/54927 [verified 15 April 2020]

Linn RR, Cunningham P (2005) Numerical simulations of grass fires using a coupled atmosphere–fire model: basic fire behavior and dependence on wind speed. *Journal of Geophysical Research, D, Atmospheres* **110**, D13107. doi:10.1029/2004JD005597

Liu N, Wu J, Chen H, Zhang L, Deng Z, Satoh K, Viegas DX, Raposo JR (2015) Upslope spread of a linear flame front over a pine needle fuel bed: the role of convection cooling. *Proceedings of the Combustion Institute* **35**, 2691–2698. doi:10.1016/J.PROCI.2014.05.100

Marsden-Smedley JB, Catchpole WR, Pyrke A (2001) Fire modelling in Tasmanian buttongrass moorlands. IV* Sustaining versus non-sustaining fires. *International Journal of Wildland Fire* **10**, 255–262. doi:10.1071/WF01026

McArthur AG (1966) Weather and grassland fire behaviour. Commonwealth of Australia, Forestry and Timber Bureau Leaflet 100. (Canberra, ACT, Australia)

McCaffrey B (1979) Purely buoyant diffusion flames: some experimental results. Report NBSIR 79–1910. U. S. Department of Commerce, National Bureau of Standards. Available at https://nvlpubs.nist.gov/nistpubs/Legacy/IR/nbsir79-1910.pdf [verified 15 April 2020].

Mell W, Maranghides A, Mcdermott R, Manzello SL (2009) Numerical simulation and experiments of burning Douglas fir trees. *Combustion and Flame* **156**, 2023–2041. doi:10.1016/J.COMBUSTFLAME.2009.06.015

Morandini F, Silvani X, Honoré D, Boutin G, Susset A, Vernet R (2014) Slope effects on the fluid dynamics of a fire spreading across a fuel bed: PIV measurements and OH chemiluminescence imaging. *Experiments in Fluids* **55**, 1788. doi:10.1007/S00348-014-1788-3

Morandini F, Silvani X, Dupuy JL, Susset A (2018) Fire spread across a sloping fuel bed: flame dynamics and heat transfers. *Combustion and Flame* **190**, 158–170. doi:10.1016/J.COMBUSTFLAME.2017.11.025

Morvan D (2011) Physical phenomena and length scales governing the behaviour of wildfires: a case for physical modelling. *Fire Technology* **47**, 437–460. doi:10.1007/S10694-010-0160-2

Morvan D (2013) Numerical study of the effect of fuel moisture content (FMC) upon the propagation of a surface fire on a flat terrain. *Fire Safety Journal* **58**, 121–131. doi:10.1016/J.FIRESAF.2013.01.010

Morvan D, Méradji S, Accary G (2009) Physical modelling of fire spread in grasslands. *Fire Safety Journal* **44**, 50–61. doi:10.1016/J.FIRESAF.2008.03.004

Morvan D, Meradji S, Mell W (2013) Interaction between head fire and backfire in grasslands. *Fire Safety Journal* **58**, 195–203. doi:10.1016/J.FIRESAF.2013.01.027

Morvan D, Accary G, Meradji S, Frangieh N, Bessonov O (2018) A 3D physical model to study the behavior of vegetation fires at laboratory scale. *Fire Safety Journal* **101**, 39–52. doi:10.1016/J.FIRESAF.2018.08.011

Nelson RM, Jr, Adkins CW (1986) Flame characteristics of wind-driven surface fires. *Canadian Journal of Forest Research* **16**, 1293–1300. doi:10.1139/X86-229

Noble IR, Gill AM, Bary GAV (1980) McArthur's fire-danger meters expressed as equations. *Australian Journal of Ecology* **5**, 201–203. doi:10.1111/J.1442-9993.1980.TB01243.X

Pagni PJ, Peterson TG (1973) Flame spread through porous fuels. *Symposium (International) on Combustion* **14**, 1099–1107. doi:10.1016/S0082-0784(73)80099-2

Perry GLW (1998) Current approaches to modelling the spread of wildland fire: a review. *Progress in Physical Geography* **22**, 222–245. doi:10.1177/030913339802200204

Rossa CG (2017) The effect of fuel moisture content on the spread rate of forest fires in the absence of wind or slope. *International Journal of Wildland Fire* **26**, 24–31. doi:10.1071/WF16049

Rossa CG, Veloso R, Fernandes PM (2016) A laboratory-based quantification of the effect of live fuel moisture content on fire spread rate. *International Journal of Wildland Fire* **25**, 569–573. doi:10.1071/WF15114

Rothermel RC (1972) A mathematical model for predicting fire spread in wildland fuels. USDA Forest Service, Intermountain Forest and Range Experiment Station, Research Paper INT-115. (Ogden, UT, USA)

Rothermel RC, Anderson HE (1966) Fire spread characteristics determined in the laboratory. USDA Forest Service, Intermountain Forest Range Experiment Station, Research Paper INT-30. (Ogden, UT, USA)

Sánchez-Monroy X, Mell W, Torres-Arenas J, Butler BW (2019) Fire spread upslope: numerical simulation of laboratory experiments. *Fire Safety Journal* **108**, 102844. doi:10.1016/J.FIRESAF.2019.102844

Sullivan AL (2009*a*) Wildland surface fire spread modelling, 1990–2007. 1: Physical and quasi-physical models. *International Journal of Wildland Fire* **18**, 349–368. doi:10.1071/WF06143

Sullivan AL (2009*b*) Wildland surface fire spread modelling, 1990–2007. 2: Empirical and quasi-empirical models. *International Journal of Wildland Fire* **18**, 369–386. doi:10.1071/WF06142

Viegas DX (2004) A mathematical model for forest fires blowup. *Combustion Science and Technology* **177**, 27–51. doi:10.1080/00102200590883624

Viegas DX, Simeoni A (2011) Eruptive behaviour of forest fires. *Fire Technology* **47**, 303–320. doi:10.1007/S10694-010-0193-6

Weber RO (1990) A model for fire propagation in arrays. *Mathematical and Computer Modelling* **13**, 95–102. doi:10.1016/0895-7177(90)90103-T

Weise DR, Koo E, Zhou X, Mahalingam S, Morandini F, Balbi JH (2016) Fire spread in chaparral – a comparison of laboratory data and model predictions in burning live fuels. *International Journal of Wildland Fire* **25**, 980–994. doi:10.1071/WF15177

Appendix A – Wind velocity

When a fire is spreading upslope over a fuel bed, it generates an indraught coming from the unburnt zone that provides convective cooling and an indraught coming from the burnt zone. A distinction is made between the three following cases:

First case: ambient wind velocity is zero

In the absence of natural wind, U is only equal to the velocity of the fire-generated inflow coming from the burnt area. This air flow enters the flame base and supplies oxygen to the flame. The quantification of this fresh indraught is derived from the ratio between air and pyrolysis gases and is assumed to be constant ($s_t = 17$):

$$\rho_a U\left(h+\frac{H}{2}\right) = s_t L\dot{\sigma}_u \tag{A1}$$

As flame thickness L is equal to the product of ROS R and flame residence time τ, and assuming that the effective mass loss rate $\dot{\sigma}_u$ is equal to the ratio between effective fuel load σ_u (see Eqn B2) and flame residence time τ, Eqn A1 yields:

$$U\left(h+\frac{H}{2}\right) = s_t \frac{R\tau}{\rho_a}\frac{\sigma_u}{\tau} \tag{A2}$$

And finally, using Eqns B3 and B5 and the definition of fuel density ρ_v ($\rho_v = \sigma/(h\beta)$),

$$U = \left(s_t \frac{h}{h+\frac{H}{2}}\frac{\rho_v}{\rho_a}\min\left(1,\frac{h}{\delta}\right)\beta\right)R \tag{A3}$$

Eqn A3 is coupled with the definition of ROS given by Eqn 28. As suggested by Viegas (2004) and Viegas and Simeoni (2011), this coupling creates a feedback effect that leads in most cases to an equilibrium value of ROS. Balbi *et al.* (2014) showed that the feedback effect may turn the fire behaviour into an eruptive fire if the terrain slope angle is greater than a threshold value. Indeed, the flame attachment described by Dold and Zinoviev (2009) involves an unsteady phenomenon conveyed by a sudden acceleration of ROS observed by Liu *et al.* (2015) with upslope spreads of a linear flame front. Balbi *et al.* (2014) provided a physical condition (which depends on meteorological conditions, topography, fuel characteristics and fire dynamics) to determine fire eruption triggering. More recently, Chatelon *et al.* (2018) improved this condition, which was successfully applied to the set of experiments carried out by Liu *et al.* (2015).

However, as the model proposed in the present paper is a simplified physical steady-state propagation model, it is not designed to model ROS during fire eruption.

Second case: ambient wind velocity is smaller than the speed of the fire-generated inflow

If the ambient wind velocity is lower than the flame-induced airflow, then ambient wind velocity is completed in order to reach the value of U.

Third case: ambient wind velocity is greater than the speed of the fire-generated inflow

The ambient wind is dominant in driving the fire dynamics.

Finally, the term U, defined in the proposed model, represents the sum of the normal (to the fire front) component of the wind velocity and the fire-induced wind velocity if ambient wind speed is lower than the fire-generated inflow and is equal to natural ambient wind velocity otherwise.

Appendix B – Upward gas velocity and mean flame temperature

Assuming that the air enters the flame in the stoichiometric proportion s_t, the vertical gas flow rate at mid-height of the flame (u_0 on flat terrain, u on sloping terrain) is equal to the sum of the pyrolysis gases flow rate ($L\dot{\sigma}_u$) and the flow rate of the fresh air absorbed by the flame ($s_t L s_t L\dot{\sigma}_u$) (Balbi *et al.* 2009):

$$\rho u\frac{L}{2}\cos\alpha = s_t L\dot{\sigma}_u + L\dot{\sigma}_u \tag{B1}$$

σ_u denotes the effective fuel load (i.e. the part of fuel load that will actually burn) and is related to the char fraction c. The modelling of the effective fuel load is the following:

$$\sigma_u = \sigma(1-c) = \sigma\frac{h_u}{h} \tag{B2}$$

where h_u is the fuel bed depth under combustion. Indeed, in the flame base, the fuel is heated by flame body radiation, which decreases as it rises vertically into the stratum. If this vegetation stratum is deep enough, δ denotes the extinction depth for which the flame radiation is close to zero. Extinction depth is related to optical depth (De Mestre *et al.* 1989) but differs by one factor. This factor is based on the shadow obtained by projection of the fuel particles on the ground and the expression of the extinction depth is the following (for a continuous and homogeneous vegetation stratum):

$$\delta = \frac{2\pi}{s\beta} \tag{B3}$$

So the fuel bed depth actually heated h_u is equal to δ if the fuel bed depth is greater than the extinction depth and is equal to h otherwise, which gives $h_u = \min(\delta,h)$, and thus:

$$\frac{h_u}{h} = \min\left(1,\frac{2\pi}{S}\right) \tag{B4}$$

where S is the leaf area ($S = s\beta h$). This ratio h_u/h represents the fuel consumption rate and, thus, the char fraction is modelled as follows:

$$c = 1-\min\left(1,\frac{2\pi}{S}\right) \tag{B5}$$

We assume that the effective mass loss rate $\dot{\sigma}_u$ is approximated by the effective fuel load/flame residence time ratio:

$$\dot{\sigma}_u = \frac{\sigma_u}{\tau} \tag{B6}$$

As Balbi *et al*. (2009) showed that $u_0 = u\cos\alpha$, a combination of Eqns B1 and B6 gives:

$$u_0 = 2\frac{s_t + 1}{\rho}\frac{\sigma_u}{\tau} \tag{B7}$$

As $\rho_a T_a = \rho T$ and with the expression of the flame residence time given by Andrews (1986), $\tau = \tau_0/s$, Eqns B7 and B2 yield:

$$u_0 = 2\frac{s_t + 1}{\rho_a}\frac{T}{T_a}\frac{s}{\tau_0}\sigma\frac{h_u}{h} \tag{B8}$$

The final expression of u_0 is obtained using the definitions of the leaf area S, the packing ratio ($\beta = \sigma/h\rho_v$) and Eqn B4:

$$u_0 = 2\frac{s_t + 1}{\tau_0}\frac{T}{T_a}\frac{\rho_v}{\rho_a}\min(S, 2\pi) \tag{B9}$$

Similarly, a thermal balance in the flame body (for a linear metre of fire front) suggests that the heat released each second by gaseous combustion denoted by $Q(Q = \Delta HL\dot{\sigma}_u)$ leads to a radiative fraction χQ:

$$\rho C_{pa} u\frac{L}{2}T\cos\alpha - (s_t + 1)LC_{pa}\dot{\sigma}T_a = (1 - \chi)Q \tag{B10}$$

As $Q = \Delta HL\dot{\sigma}_u$, after simplification, the combination of Eqns B10 and B1 yields the expression for mean flame temperature:

$$T = T_a + \frac{\Delta H(1 - \chi)}{(s_t + 1)C_{pa}} \tag{B11}$$

Appendix C – radiative heat contribution

Eqn 14 gives the expression for the radiant heat flux under the flame. The first integral represents the radiant heat flux density impinging on a point M (belonging to the segment [BD]). Calculation of this integral leads to:

$$\frac{1}{\pi}\int_{ABI}\frac{\cos\varphi_1\cos\varphi_2}{d^2}d\sum = \frac{1}{2}(1 - \cos\theta) \tag{C1}$$

where θ is the view angle of the flame from point M.

The second integral in Eqn 14 can be written (after some intermediate calculations):

$$\int_D^B \frac{1}{2}(1 - \cos\theta)dx = \frac{l}{2}(1 + \sin\gamma - \cos\gamma) \tag{C2}$$

where l and γ represent flame length and flame tilt angle respectively.

Then, Eqns C2 and 14 yield:

$$\phi_r = \varepsilon BT^4\frac{l}{2}(1 + \sin\gamma - \cos\gamma) \tag{C3}$$

According to Balbi *et al*. (2007), the power emitted by an infinite radiant panel depends on the radiative fraction χ and the total flame energy:

$$l\varepsilon BT^4 = \frac{\chi}{2}\Delta HL\dot{\sigma} \tag{C4}$$

McCaffrey (1979) emphasised that the radiative fraction decreases with the volume/surface ratio of the flame and, if χ_0, V_f and S_f respectively denote a radiance coefficient, flame volume and flame surface area, Balbi *et al*. (2009) convey its expression as:

$$\chi = \frac{\chi_0}{1 + p\frac{V_f}{S_f}} \tag{C5}$$

where p denotes a proportionality coefficient.

If H^*, L and l respectively denote flame height (normal to the ground), flame depth and flame length, simple calculus (based on triangular flame geometry; see Fig. 2) leads to:

$$\frac{V_f}{S_f} = \frac{\frac{1}{2}H^* L}{l} \tag{C6}$$

combining $l = H^*/\cos\gamma$ (see Fig. 2) and $L = R\tau$ gives $L = R\tau_0/s$ (using the law for flame residence time used in BEHAVE; Andrews 1986). So, Eqn C5 yields

$$\chi = \frac{\chi_0}{1 + p\frac{R\tau_0\cos\gamma}{2s}} \tag{C7}$$

Combining Eqns C4 and C7 yields

$$l\varepsilon BT^4 = \frac{1}{2}\frac{\chi_0}{1 + p\frac{R\tau_0\cos\gamma}{2s}}\Delta H\, R\tau\frac{\sigma}{\tau} \tag{C8}$$

Defining $r_{00} = 2/(p\tau_0)$, Eqns 8 and 14 give:

$$R_r = \frac{a_r}{\sigma q}\frac{\chi_0}{1 + \frac{R\cos\gamma}{sr_{00}}}\Delta H\, R\sigma\frac{1}{4}(1 + \sin\gamma - \cos\gamma) \tag{C9}$$

which can be rewritten as in Eqns 15 and 16:

$$R_r = AR\frac{(1 + \sin\gamma - \cos\gamma)}{1 + \frac{R\cos\gamma}{sr_{00}}}\ \text{with}\ A = \frac{a_r\chi_0\Delta H}{4q}$$

The flame tilt angle γ is computed using Eqn 2.

Appendix D – Determination of airflow velocity inside flame base

Eqns 19 and 20 yield:

$$U(L) = U\,exp\left(-K_1^* s\,\beta^{\frac{1}{2}}L\right) \tag{D1}$$

As flame base depth L is equal to the product of ROS and flame residence time τ ($L = R\tau$), and using the expression for

flame residence time given by Andrews (1986) in BEHAVE ($\tau = \tau_0/s$), Eqn D1 yields:

$$U(L) = U\,exp\left(-K_1^{*}\,s\,\beta^{\frac{1}{2}}\,R\,\frac{\tau_0}{s}\right) \tag{D2}$$

Setting the drag coefficient $K_1 = K_1{}^{*}\tau_0$, Eqn 21 is finally obtained from Eqn D2.

Appendix E – Convective heat contribution

The convective heat flux depends on fuel thickness (h) and extinction depth (δ). Indeed, if the fuel thickness is smaller than the extinction depth, the convective heat flux is defined by:

$$\phi_c = \Delta H L \dot{\sigma}\,\frac{Area(BB_0F)}{Area(ABB_0A_0)} = \Delta H L \dot{\sigma}\,\frac{h^2\tan\gamma_c}{2hL} \tag{E1}$$

Assuming that the mass loss rate is practically σ/τ and as $L = R\tau$ with $\tau = \tau_0/s$ (Andrews 1986), Eqn E1 yields:

$$\phi_c = \frac{\Delta H}{2\tau_0}\sigma s h\,\tan\gamma_c \tag{E2}$$

If the fuel thickness is greater than the extinction depth, Eqns E1 and E2 can be written with δ instead of h:

$$\phi_c = \frac{\Delta H}{2\tau_0}\sigma s \delta\,\tan\gamma_c \tag{E3}$$

Finally, Eqns E2 and E3 give the expression of the convective heat flux (Eqn 25).

The contribution of convective effects to ROS is given by Eqn 7. Combining Eqns 7, 25 and 26 yields:

$$R_c = \frac{h}{h+\frac{H}{2}}\frac{\Delta H}{2q\sigma\tau_0}\sigma s\,\min(h,\delta)\,\tan\gamma_c \tag{E4}$$

Substituting extinction depth δ and tan γ_c with their expressions (Eqn 12 and 18 respectively) gives:

$$R_c = \frac{h}{h+\frac{H}{2}}\frac{\Delta H}{2q\tau_0}s\,\min\left(h,\frac{2\pi}{s\beta}\right)\left(\tan\alpha + \frac{U(L)}{u_c}\right) \tag{E5}$$

Using Eqns 21 and 22:

$$R_c = \frac{h}{h+\frac{H}{2}}\frac{\Delta H}{2q\tau_0}s\,\min\left(h,\frac{2\pi}{s\beta}\right)\left(\tan\alpha + \frac{U\,exp\left(-K_1\beta^{\frac{1}{2}}R\right)}{\frac{h}{h+\frac{H}{2}}\frac{u_o}{2}}\right) \tag{E6}$$

The contribution of convective effects to ROS (Eqn 27) is finally obtained by expanding Eqn E6.